# OSSOS. XIV. The Plane of the Kuiper Belt

Christa van Laerhoven, Brett Gladman, Kathryn Volk, J. J. Kavelaars, Jean-Marc C. Petit, Michele T. Bannister, Mike Alexandersen, Ying-Tung Chen, Stephen D. J. Gwyn

Draft version April 12, 2019
Typeset using LaTeX **preprint** style in AASTeX62

# OSSOS: XIV. The Plane of the Kuiper Belt

Christa Van Laerhoven,[1] Brett Gladman,[1] Kathryn Volk,[2] J. J. Kavelaars,[3,4] Jean-Marc Petit,[5] Michele T. Bannister,[6] Mike Alexandersen,[7] Ying-Tung Chen (陳英同),[7] and Stephen D. J. Gwyn[4]

[1] *University of British Columbia, 6224 Agricultural Road, Vancouver, BC V6T 1Z1, Canada*
[2] *Lunar and Planetary Laboratory, 1629 E University Blvd, Tucson, AZ 85721-0092, USA*
[3] *Department of Physics and Astronomy, University of Victoria, Elliott Building, 3800 Finnerty Rd, Victoria, BC V8P 5C2, Canada*
[4] *Herzberg Astronomy and Astrophysics Research Centre, National Research Council of Canada, 5071 West Saanich Rd, Victoria, British Columbia V9E 2E7, Canada*
[5] *Institut UTINAM UMR6213, CNRS, Univ. Bourgogne Franche-Comté, OSU Theta F25000 Besançon, France*
[6] *Astrophysics Research Centre, School of Mathematics and Physics, Queen's University Belfast, Belfast BT7 1NN, United Kingdom*
[7] *Institute of Astronomy and Astrophysics, Academia Sinica; 11F of AS/NTU Astronomy-Mathematics Building, Nr. 1 Roosevelt Rd., Sec. 4, Taipei 10617, Taiwan*

## ABSTRACT

The orbits of Solar System objects are subject to external perturbations by other massive bodies and slowly precess about a forced (averaged) plane. Warps in the plane come from the effects of the total planetary system, so discrepancies from expectation can show the presence of any unseen planets. We investigate the orbital inclination distribution from 42.4 au to 150 au with the non-resonant trans-Neptunian discoveries and the survey simulator of the Outer Solar System Origins Survey (OSSOS). We statistically determine local forced planes and the widths of the populations' inclination distributions. Between the $\nu_{18}$ and the 2:1 resonance at 47.5 au, the derived forced plane and the expected forced plane (from secular perturbations due to the known planets) match very well. As in previous studies, we reject the ecliptic as the forced plane. We also reject the invariable plane inside of 44.4 au beyond which the forced plane starts approaching the invariable plane. From 44.4 au to 150 au the forced plane is consistent with the invariable plane, as expected based on the known planets. The dynamically cold Kuiper Belt (between the $\nu_{18}$ and the 2:1 resonance) is best fit with a free inclination width of only $\simeq 1.75°$, strongly limiting its past perturbation. The dynamically excited populations have broader inclination distributions: the hot Kuiper Belt is $\simeq 14°$ wide, and non-resonant orbits in the semimajor axis range beyond the 2:1 resonance out to 150 au have an inclination width of $\simeq 17°$. The OSSOS data does not strengthen claims of present additional Mars-mass planets within $\sim 100$ au.

Corresponding author: Christa Van Laerhoven
cvl@phas.ubc.ca, c.vanlaerhoven@gmail.com

*Keywords:* solar system — Kuiper Belt — dynamics — surveys

## 1. INTRODUCTION

Heliocentric keplerian orbits precess due to the small perturbations that are exerted by planetary bodies, which results in orbits that do not close. For small perturbations, one aspect of this precession is that each small-body orbital pole (angular momentum vector) precesses at a constant inclination relative to a local 'Laplace pole', where the Laplace pole steadily changes as a function of orbital semimajor axis. This 'Laplace pole' is the vector about which the small-body's angular momentum vector will precess. Equivalently, one can talk about the 'forced plane', the plane perpendicular to the Laplace pole. If all the planetary masses and orbits are known, one can compute the expected position of the local Laplace pole. Inversely, if one is able to determine via bias-free observation of small bodies what pole they are symmetrically distributed about, one can empirically find the local Laplace pole. Lastly, if one can do both, then a disagreement between the expected pole and the empirical symmetric pole from observations would detect the presence of an unseen mass (or masses) that are perturbing the heliocentric orbits. In addition, the *dispersion* of orbital inclinations, relative to this pole, yields information on the processes that have excited random velocities in the small-body population.

In the trans-Neptunian Kuiper Belt, the limiting case (once one is far beyond all the planetary orbits) is that the small-body Laplace pole is the total angular momentum vector of the planetary system. The plane perpendicular to this, in which small body orbits would precess in perihelion direction but maintain a constant zero relative inclination, is called the invariable plane. As one approaches the planetary system, the Laplace pole position steadily moves, in a way that is calculable via standard Laplace-Lagrange secular perturbation theory (see Section 2.1).

Unfortunately, it is not possible to simply take all observational data of known trans-Neptunian objects (TNOs) and average them to find the center of the distribution (though, such a process is possible for the Asteroid Belt, see Saverio & Malhotra 2018). This is because any telescopic survey with a small range of ecliptic latitude and longitude is strongly biased towards detecting only a subset of all possible orbital inclinations and ascending nodes. Concluding the actual forced plane would thus require very precise understanding of survey performance: detection efficiency as a function of depth in magnitudes, for each examined region of sky. Brown & Pan (2004) proposed a method to try and counter the observational biases and applied it to the Kuiper Belt as a whole, finding an 'averaged Kuiper Belt plane' that was distinct from the invariable plane — as expected by a sample of TNOs dominated by objects with semimajor axes in the range 42–47 au (due to the influence of the $\nu_{18}$ secular resonance, see Section 2.1). COUPLE SENTENCES DESCRIBING BROWN AND PAN METHOD HERE? Elliot et al. (2005) applied several other methods to a larger TNO sample. They derived a different result for the entire Kuiper Belt, but pointed out it was necessary to eventually interpret these results on smaller sub-samples, because the forced plane is semimajor axis dependent; using only the objects of the 'classical belt' matched the expected secular location. Chiang & Choi (2008) used a restricted TNO sub-sample at two narrow semimajor ranges (near $a = 38$ au and $a = 43$ au) to demonstrate that the several degree difference in the forced plane location for these two semimajor axes was detectable. Most recently, Volk et al. (2017) calculated the mean plane of

non-resonant TNOs from the Minor Planet Center[1] catalog, using the Brown & Pan (2004) method on all objects available in the worldwide sample by this time, and found that most of the Kuiper Belt follows what is expected from Laplace-Lagrange secular theory. However, for semimajor axes $a$=50–80 au the method indicated that the forced plane was not the (expected) invariable plane, at more than 95% confidence. Their analysis indicated that the forced plane was instead offset by $\sim 9^\circ$ in a particular direction. This departure would be evidence for non-negligible mass in this region of the Solar System.

Some of the assumptions inherent in these approximate methods (for example, needing to assume the inclination distribution rather than fitting for it) can be avoided if one uses a characterized survey. In this paper we use the Outer Solar System Origins Survey (OSSOS), a well characterized survey of 155 square degrees to limiting magnitudes in the range $m_r$ =24-25, which tracked all TNOs discovered in the survey to avoid tracking biases (Bannister et al. 2018). When discussing the outer trans-Neptunian belt we supplement OSSOS with characterized TNOs from CFEPS (Petit et al. 2011), HiLat (Petit et al. 2017)), and Alexandersen et al. (2016). A characterized survey can assess both the detection and *non-detection* of objects. It is thus a powerful tool in constraining allowed mean planes. For any hypothesised trans-Neptunian belt, one can determine if that hypothesised belt would result in detection of abundant numbers of TNOs with ascending nodes at a certain longitude. If such objects are not detected by the calibrated surveys then that hypothesised trans-Neptunian belt can be rejected. A characterized survey that reports all of its detections is also free from 'reporting bias', where incomplete reporting of all detections can skew the derived forced plane. In order to understand the expected signal of the forced plane in a characterized survey, we first briefly review how secular perturbations affect small bodies in the outer Solar System. We then explain how we compare detected TNOs from calibrated surveys with models of various portions of the trans-Neptunian belt, to determine if we find any departures from the theoretical expectation.

## 2. METHODS

### 2.1. *The Expected Plane from Secular Theory*

The orientation of an orbital plane is described via the inclination ($i$) and the longitude of ascending node ($\Omega$). The inclination sets how tilted the orbit is from the reference plane, and the longitude of ascending node describes where the orbital plane and reference plane intersect. Often it is more convenient to describe the orientation of the orbital plane via the rectangular coordinates

$$q = \sin i \cos \Omega \quad (1)$$

$$p = \sin i \sin \Omega \quad (2)$$

where $i$ is the inclination and $\Omega$ is the longitude of ascending node, which we will reference to the J2000 ecliptic coordinate system. $q$ and $p$ are defined only on the interval [-1,1]. (The reader should note that that while $q$ and $p$ are defined with $\sin i$ dependence on the inclination, most figures in this paper use $i \cos \Omega$ and $i \sin \Omega$ as coordinates for ease of interpretation.)

In a multi-body system, the inclinations of any given body are not constant. The massive bodies exchange angular momentum and their inclinations change. Any massless test particle has an inclination that is the vector sum of an inclination forced by the massive bodies, and a free inclination.

[1] https://www.minorplanetcenter.net/

According to classical second-order secular theory (Murray & Dermott 1999) the forced inclination of a massless test particle is

$$(q_0, p_0) = (\sin i_0 \cos \Omega_0, \ \sin i_0 \sin \Omega_0) \tag{3}$$

$$= \sum_{i=1}^{8} \frac{\mu_i}{f_i - f_0} (\ \cos(f_i t + \gamma_i), \ \sin(f_i t + \gamma_i)\ ) \tag{4}$$

where $f_0$ is the nodal precession rate of the test particle, $f_i$ are the planetary system's secular inclination eigenfrequencies, $\gamma_i$ are the eigenmode phases, and $\mu_i$ is a weighting factor for each secular eigenmode. The secular eigenfrequencies, $f_i$, depend only on the masses and semi-major axes of the eight major planets and the mass of the sun. These frequencies are essentially the natural frequencies of the planetary system. The inclinations of the massive bodies vary with these frequencies. The test particle's nodal precession frequency, $f_0$, involves the masses and semi-major axes of the planets and additionally the semi-major axis of the test particle (once its eccentricity, $e$, and inclination,$i$, become sufficiently large, the test particle's precession rate can also depend on its own $e$ and $i$). (Note that the subscript 0 refers to the test particle.) The eigenmode phases, $\gamma_i$, depend on the planet masses, semi-major axes, inclinations and nodes. The weighting factors, $\mu_i$, depend on all of the planetary parameters (masses, semi-major axes, inclinations, and ascending nodes) and also the test particle's semi-major axis.

The free inclination represents residual vertical motions relative to the local forced plane. If an object has no free inclination its orbit resides in the forced plane. If an object does have a non-zero free inclination that object will precess about the forced plane at its nodal precession rate $f_0$. For any given semi-major axis, the average of many objects' orbital planes, or the long-term average orbital plane of a single object will be the forced plane.

Figure 1 shows how $q_0$ and $p_0$ vary as a function of the test particle's semi-major axis, using planetary inclination information from Murray & Dermott (1999). At large semi-major axes ($q_0$,$p_0$) converges to the invariable plane (the total angular momentum plane of the solar system). But at 35 and 40.3 au the expected forced plane is strongly warped due to secular resonance. These are places where $f_0$, essentially the test particle's natural frequency, is very similar to one of the secular frequencies ($f_i$).

Note that the forced plane has a time dependence. Like the inclination vectors of the planets themselves, the forced inclination of a test particle is a vector sum of contributions from the secular inclination eigenmodes, which each rotate in ($q$,$p$) space. The test particle also generally has a free inclination that adds another vector to this vector sum. Thus, the (total) inclination of a test particle will oscillate around the forced inclination, which in turn will ultimately oscillate around the invariable plane.

### 2.2. *Survey Simulation*

If all Kuiper Belt objects were known, then the symmetry center of all objects in $(q, p)$ space would correspond to the current forcing plane. However, surveys of the Kuiper Belt can only provide an observationally biased subset of the population, introducing effects which skew the derived plane (Brown & Pan 2004; Volk et al. 2017). Any given survey only points in certain directions, only detects objects to a certain limiting magnitude, only looks for objects that move at certain rates,

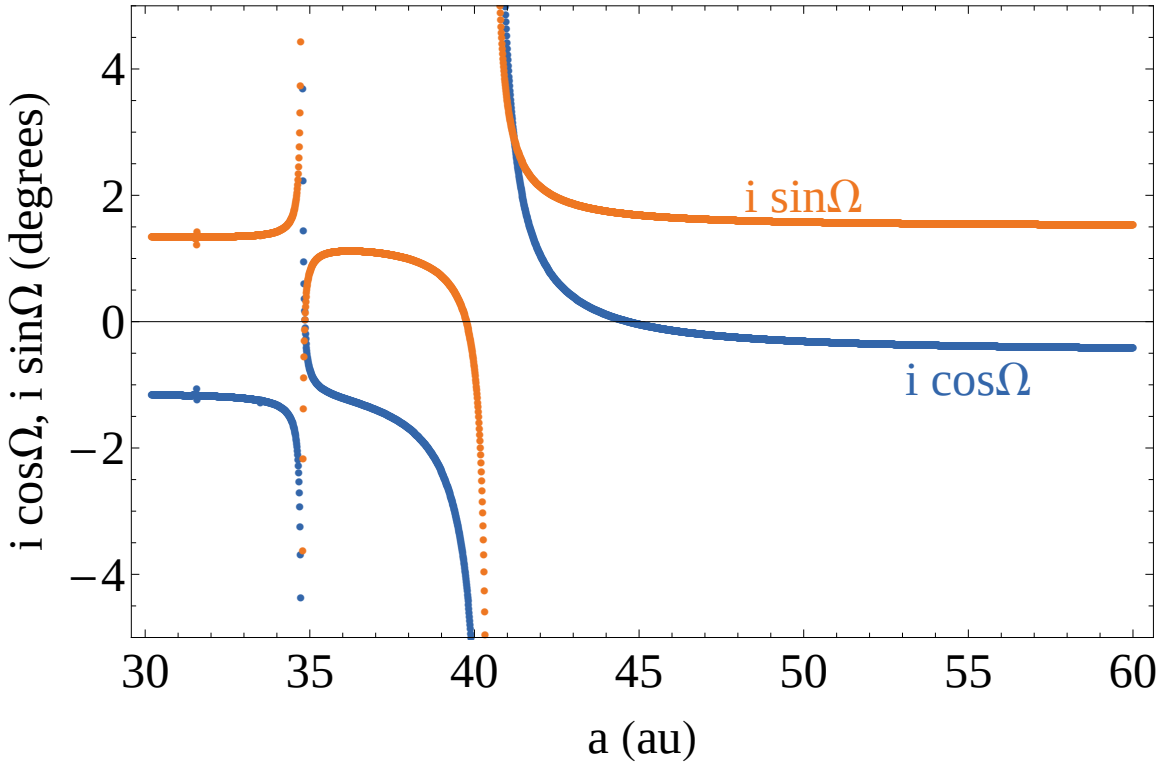


**Figure 1.** The expected forced $i_0 \cos \Omega_0$ (blue) and $i_0 \sin \Omega_0$ (orange) of a test particle as a function of its semi-major axis, given the 8 known planets (from Eqn 4). The features evident at $a \approx$34.8 and 40.5 au are caused by secular resonances with the planetary system. The large-$a$ limit is the invariable plane, with $(i_I \cos \Omega_I, i_I \sin \Omega_I)$ and $i_I = 1.578^o$ and $\Omega_I = 107.58^o$ in J2000 ecliptic coordinates.

and then any given object might not be recovered by subsequent observations (i.e. be 'lost'). Most of the detections available in the compilation of TNOs in the IAU Minor Planet Center cannot be tied to a survey for which detection efficiency as a function of orbit and absolute magnitude could be calculated. However, 'characterized' surveys (Petit et al. 2011; Jones et al. 2006) provide the information which allows one to compute if an object with given orbit and absolute magnitude would be visible in a survey (or at least a probability of detection as a function of the resulting apparent magnitude on an observation date where the object is in the field). Use of a 'survey simulator' (Petit et al. 2011; Lawler et al. 2018) then enables direct comparison of a model trans-Neptunian belt to the real observed trans-Neptunian objects.

Our primary characterized survey is OSSOS, whose 838 characterized detections are by far the largest characterized set available for study (Bannister et al. 2018). This survey provides a huge number of non-resonant TNOs, with orbits measured at higher precision than most in the MPC, and completely dominates the statistics for our studies of the main classical Kuiper Belt. We consider only the single-color $r$ band survey of OSSOS for the main trans-Neptunian belt as including other characterized surveys adds complications (e.g. making assumptions about TNO colors), while not significantly affecting the results.

Because we know the sky coverage of each group of survey pointings along with the probability of detection as a function of TNO magnitude and rate of motion, we can evaluate the probability of detecting any given TNO. Repeating this evaluation over very large number of simulated objects

drawn from a specified underlying distribution builds up the population of 'simulated detections'. These simulated detections can then be compared to the real OSSOS detections, to ascertain whether the proposed trans-Neptunian belt is consistent with the real trans-Neptunian belt.

Beyond $a$=50 au, however, the wide distribution of inclinations (Gulbis et al. 2010; Petit et al. 2017) and lower overall detection frequency (due to their more distant orbits) results in in fewer detected objects in the invariable-plane-focused sky coverage of OSSOS, and better statistics are required. We supplement OSSOS detections in $a > 50$ au with those of three smaller characterized surveys:

- The Canada-France Ecliptic Plane survey (CFEPS), which is a wider but shallower survey mostly in $g$ band near the ecliptic (Petit et al. 2011);
- The CFEPS High Latitude extension (HiLat, Petit et al. 2017), which explored the sky away from the ecliptic, to strongly constrain the form of the tail of the inclination distribution;
- The study of Alexandersen et al. (2016), which targeted the near-ecliptic sky ahead of Neptune to maximize detections of leading Neptune trojans and Plutinos.

All of these works provide the information needed to do the modelling described herein. The earlier survey of Schwamb et al. (2010) would provide a small number of additional $a > 50$ au non-resonant TNOs, but as it has a comparatively low-precision detection efficiency function, we elected not to incorporate it.

The orbital distribution models we use here can remain simple, as our testing showed that the results were largely insensitive to assumptions about the orbital distributions, outside the parameter space of orbital inclination and longitude of ascending node. Because we are trying to constrain the distribution of orbital planes (or, equivalently, angular momentum unit vectors), major changes in semi-major axis distribution, orbital eccentricity and argument of perihelion made only tiny differences to the simulated distribution of detected nodes and orbital inclinations. We always assumed that the mean anomalies were uniformly distributed, and that the nodal longitudes were uniformly distributed in angle around the hypothesized forced plane. Because it continues to provide adequate fits to the observational data, we use the common parameterization of the inclination distribution (Brown 2001; Kavelaars et al. 2009; Petit et al. 2011; Gulbis et al. 2010; Petit et al. 2017) which has the probability density function

$$f(i) = \sin i \, \frac{1}{\sqrt{2\pi\sigma}} \, e^{-i^2/(2\sigma^2)} \, , \tag{5}$$

with the width $\sigma$ thus being the only parameter. Figure 2 shows example inclination distributions for different widths. While this formulation may not be reality, the data as yet provide no compelling reason to move to something else.

We have confirmed that assumptions about the absolute magnitude ($H_r$) distribution make little difference to our results. This is not surprising, because the largest physical effect for in- or near-plane surveys like OSSOS is simply whether the ascending node is in the direction of the survey or 180 degrees away (for objects at their descending node in the survey). For most of our studies we used a single exponential distribution with $dN \propto 10^{\alpha H}$ with $\alpha$=0.8, but we also tested in several cases that our conclusions about the forced plane did not change if we used the best fit 'knee' distribution from Lawler et al. (2018) in which $\alpha$=0.9 for $H_r < 7.7$ and $\alpha$=0.4 above.

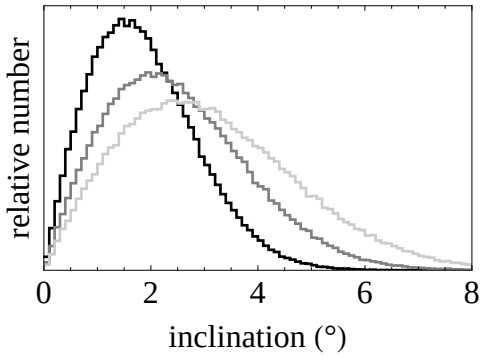


**Figure 2.** Examples of inclination distributions generated by the survey simulator, of the functional form $\sin i$ times a Gaussian (Eqn 5). The black, grey, and light grey distributions have widths of 1.5, 2.0, 2.5 degrees, respectively.

In this paper we compare the real detections from the survey (or surveys) being simulated to the population of simulated detections via a bootstrapped Kolmogorov-Smirnov (KS) statistic. (We also computed the Anderson-Darling (AD) statistics, and got similar results, so we do not present this less-familiar statistic). For every survey simulation we generate 15000 simulated detections. Of these we randomly pick out a sample equal to the number of real detections, and compare the KS statistic of the real TNOs to the KS statistic of the simulated-detected subsample for each of the $q$, $p$, $i$, and $\Omega$ cumulative distributions. The distribution of this boot-strapped statistic provides 95% and 99% confidence ranges with which the rejectability of the *real* sample can then be judged. Because $q$ and $p$ are defined on the interval $[-1, 1]$ and the signal is 'in the middle' of this range, the KS test is well adapted to these variables. Because *both* the $q$ and $p$ distributions need to be non rejectable, we construct a single 'joint' statistic for any given comparison by taking the most rejectable of these two 1-D distributions. (This is because a distribution which is fine in one variable but terrible in the other should be rejected by the joint test, and we found that the 'worst of the two' approach gave the most sensible answers when we examined the distributions of the dynamical variables). We thus extract random subsamples 3000 times and compute the joint $q, p$ statistic of that sample relative to the entire simulated sample, in order to create the bootstrap. If the joint KS value of the real sample (relative to the entire simulated detection sample from that assumed model) is beyond 95%/99% of the bootstrap KS values, we reject that model at 95% or 99% significance, respectively.

In principle, the $q, p$ distributions should contain the same information as the $i, \Omega$ distributions. However, the KS test is best at discerning how different the centers of the compared distributions are. Thus, expressing the orbit planes in terms of $q, p$ versus $i, \Omega$ can yield slightly different results for the bootstrapped KS statistic. In particular, $q, p$ are good at locating what $q, p$ are allowed as forced planes, while $i, \Omega$ provides information on whether the distribution of TNOs in $q, p$ space is too narrowly or widely concentrated. For example, this difference appears in Figure 3 versus Figure 4.

## 3. THE MAIN BELT

In this section we concentrate on the 'main belt' between the 3:2 and 2:1 resonances with Neptune, seeking to determine if the true forced plane is consistent with the expected forced plane from secular theory and to determine what the width of the inclination distribution is for the dynamically 'cold' and 'hot' populations.

Because the forced plane location is semi-major axis dependent (Fig. 1) the comparison of the real sample to the theoretical prediction is most easily done after binning the objects by orbital $a$. In previous studies, workers have chosen for their semimajor axis bins either small ranges around important values of $a$ to illustrate the secular effect (Chiang & Choi 2008), essentially no bins at all (Brown & Pan 2004), or a combination of divisions based on the secular structure and round numbers (Volk et al. 2017). Because the data set is now larger, we are able to study the variation of the plane with $a$ and have elected to use dynamical structures observed in the main-belt's semi-major axis distribution to set the semi-major axis bins, and we also separate the dynamically 'hot' and 'cold' populations (how these populations are separated is discussed in detail below). Because the values of $a$ and $e$ have only a small effect on detectability on either side of any bin boundary, the divisions we chose make no real influence on the conclusions.

Several previous studies have investigated what the mean plane and inclination widths of the main belt's subpopulations. Brown (2001) showed that the inclination distribution could be reasonably represented by two dominant components, each of Eq. 5's form, (around the *ecliptic* in that paper) with a 'cold' component of width 2.2° and a hot component of width 18°. Brown & Pan (2004) derive that the inclination width of the 'classical belt' (with no precise orbital element range supplied) is 1.3° and 12.0° for the cold and hot components. They referred all objects' inclinations to a 'Kuiper Belt plane' that they calculated and after debiasing the objects with respect to that plane using the Brown (2001) method. Elliot et al. (2005) do not derive inclination widths, but derive mean planes for a variety of subsets of the TNO population detected in the Deep Ecliptic Survey (DES), with wide semi-major axis bins which are centered in the range ∼40–45 au. Their results disagree with the 'Kuiper belt plane' calculated by Brown & Pan (2004) at the roughly 2 sigma level. (Adams et al. (2014) do derive inclination widths for the DES.) Gulbis et al. (2010) find a cold width of 2.0±0.5° upon further analysis of the DES data set. Volk et al. (2017) showed how the mean plane in the main-belt region appears to follow the expected secular solution, pointing out that the Brown & Pan (2004) method requires an assumption on the widths to estimate uncertainties in the derived mean plane. In this context, we seek to provide an independent analysis of the main-belt region's forced plane using the almost entirely independent OSSOS sample, while using a method that is directly sensitive to the inclination widths.

For the semi-major axis bins, we have elected to use the the knowledge of the cold main-belt's substructure discovered in CFEPS (Petit et al. 2011) and confirmed by OSSOS (Bannister et al. 2016). Specifically, between the 3:2 and 2:1 resonances the cold belt has discernible $(a, e)$ substructure with a concentrated 'kernel' from 43.8 to 44.4 au superposed on a wider 'stirred' population from 42.4 to 47.0 au (see below how this is used in a study of how the forced plane moves with semimajor axis). Thus, for the 'cold' component we split the region into three bins: 42.4 – 43.8 au, 43.8 – 44.4 au, and 44.4 – 47 au. For the 'hot' cosmogonic component of the main belt, we lump all objects into one bin spanning 42.4 – 47.0 au. Here the much larger inclination width means that the expected change in the forced plane position over the classical belt's semi-major axis range is only a small fraction of the inclination width.

### 3.1. *The Cold Population*

Because in the main classical Kuiper Belt both the cold and hot populations coexist as two overlapping components in parameter space, to study the cold population we first need to isolate it somehow in the observed sample. At low inclinations the cold component will dominate and at high inclinations

the hot population will dominate, but no simple $i$ cut can perfectly separate the populations. Adding compositional information (which can be revealed through observations of a TNO in multiple color filters) can aid in distinguishing unique components (e.g. Pike et al. 2017), but only the brightest $\sim 10\%$ of OSSOS discoveries yet have additional colour observations (Schwamb et al. 2018). Here we segregate the 'cold component' by considering only objects within $4^o$ of *each* proposed forced plane. This is equivalent to limiting ourselves to objects with free inclinations $< 4^o$ relative to each proposed forced plane. With such a cut, we will get very few interlopers from a hot population. We also tried a cut of $5^o$ and found substantially similar results. Our choice of cut is motivated by Dawson & Murray-Clay (2012) Figure 2, showing contamination of the cold population by the hot population as a function of inclination cut.

The location of the forced plane moves over this range of semimajor axes, so we split the sample into a number of semi-major axis bins. As discussed above, we have chosen to split the main belt into three semimajor axis bins: 42.4 – 43.8 au, 43.8 – 44.4 au, and 44.4 – 47 au. Because we cut in inclination relative to each hypothetical forced plane, the number of real objects we compare to each survey simulated sample will depend on forced plane as well as the semimajor axis bin. Assuming the forced plane is that expected from secular theory, the aforementioned bins have 107, 82, and 67 real cold ($i_{free} < 4^o$) objects.

#### 3.1.1. *The Forced Plane*

From Figures 3 and 4, we can see that most of the forced planes we tested are rejectable (white boxes in these figures are rejected at 99% confidence). Only a confined region around the expected secularly forced plane is steadily consistent with the observed OSSOS sample. The only case where the expected secularly forced plane becomes rejectable is if the width of the inclination distribution ($\sigma$) is too narrow or too wide, as tested by the $i$,$\Omega$ distribution (Figure 4). (Exactly what inclination widths are allowed depends on the semimajor axis bin, details of which are discussed in the next section.)

In the 42.4 – 43.8 au and 43.8 – 44.4 au semi-major axis ranges, the allowed (non-rejectable) values for the forced plane cluster in $q, p$ space around the expected $q_0, p_0$ from secular theory, while both the ecliptic plane and invariable plane are rejected for all inclination widths. At these semimajor axes, the difference between the expected forced plane and the invariable plane is due to the influence of the $\nu_{18}$ secular resonance. In the 44.4 – 47 au range the forced plane (and the inclination width, $\sigma$) is less constrained due to fewer $i_{free} < 4$ objects. Here, the invariable plane is not rejectable, but in this region the expected secularly forced plane is not so different from the invariable plane since as semi-major axis increases the secularly forced plane approaches the invariable plane (Figure 1).

Overall, we agree with Volk et al. (2017) that the main Kuiper Belt nicely follows the expected secularly forced plane. Volk et al. (2017) note that in their two (overlapping) outermost bins in this region they see a weak discrepancy from the expected forced plane. While we do not see such a discrepancy, disagreements of this weak statistical significance are reasonable when comparing results from two independent data sets.

#### 3.1.2. *The Width of the Cold Inclination Distribution*

Previous understanding of the inclination distribution was achieved by finding widths of the distribution that were non-rejectable (Petit et al. 2011; Gulbis et al. 2010). There were simply too few

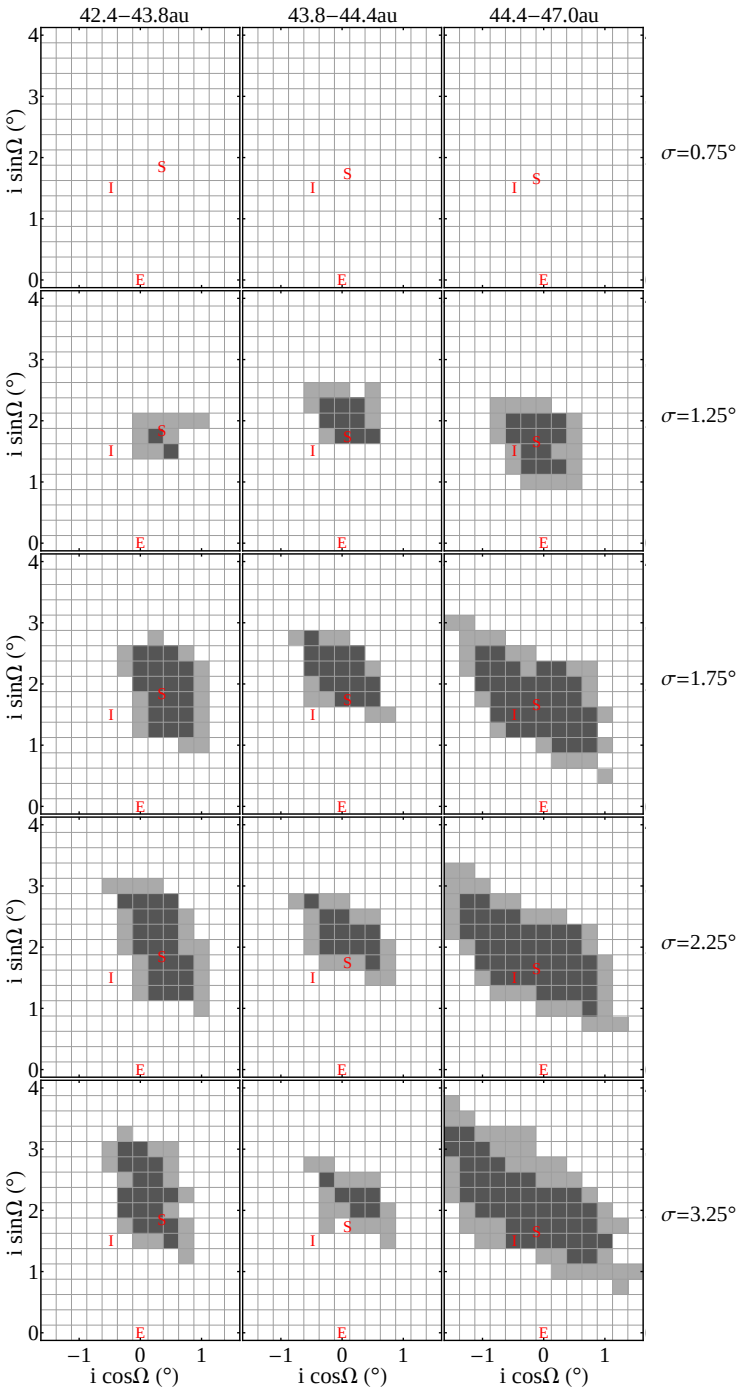


**Figure 3.** Joint bootstrapped KS statistic for the $q, p$ distributions, for different semi-major axis bins (columns), width of the inclination distribution (rows), and forced planes ($i\cos\Omega$,$i\sin\Omega$). Any bootstrapped statistic above 0.05 displays as dark grey, bootstrapped statistics between 0.05 and 0.01 are light grey (i.e. 95% and 99% confidence limits, respectively). The red E, I, and S denote the ecliptic, invariable, and expected secular forced plane, respectively. The displayed S is the expected forced plane for a TNO with semimajor axis at the mid point of each semimajor axis bin. Note that because of dependence on TNO semimajor axis (Eqn 4) the location of S is different in the different semimajor axis ranges, and also within each semimajor axis range.

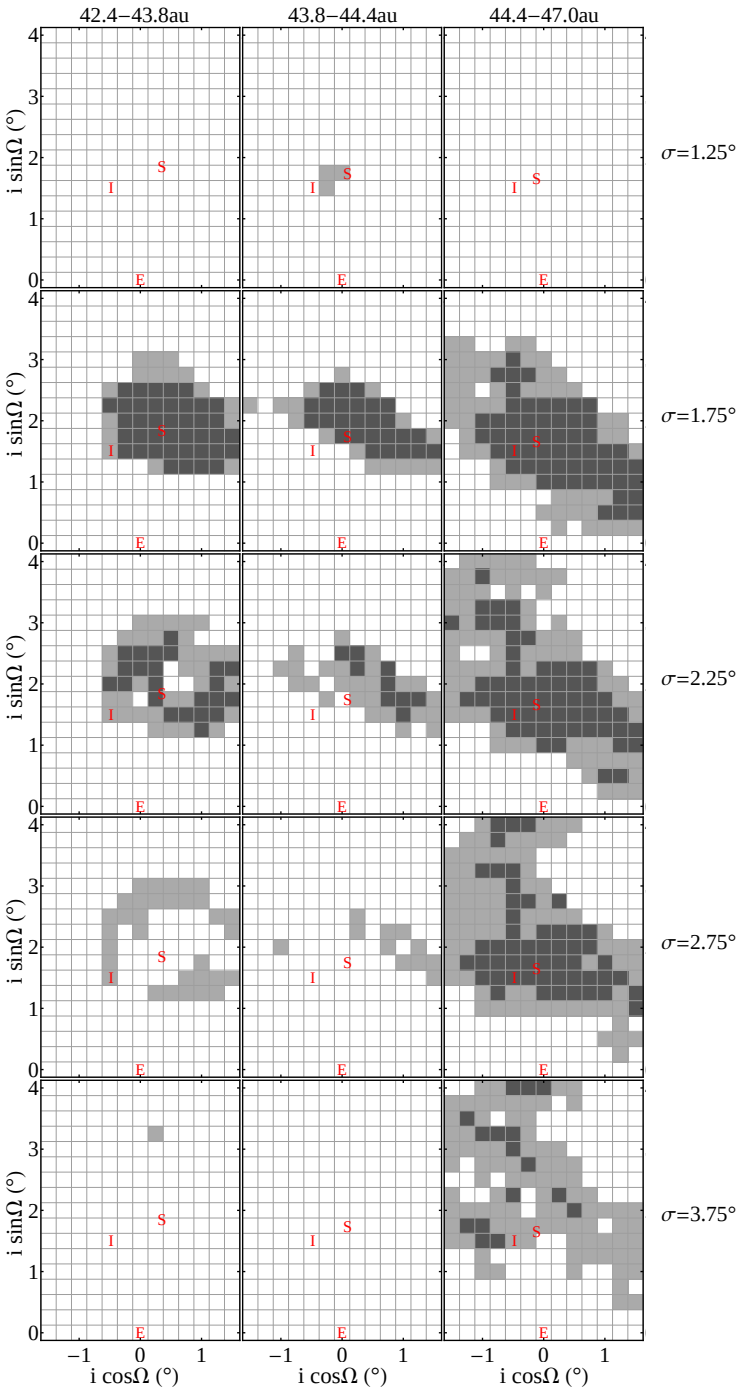


**Figure 4.** Joint bootstrapped KS statistic for the $i, \Omega$ distributions, for different semi-major axis bins (columns), width of the inclination distribution (rows), and forced planes ($i\cos\Omega$,$i\sin\Omega$), c.f. Figure 3. Note that the values of $\sigma$ shown (rows) are different in this figure versus Figure 3. Not obvious from the diagram is that the inclination distribution is much more sensitive than the node ($\Omega$) distribution. That is, the boundary between rejected and not-rejected is usually caused by the $i$ distribution being rejectable or non-rejectable, the $\Omega$ distribution is more permissive (see the text in Section 3.1.2).

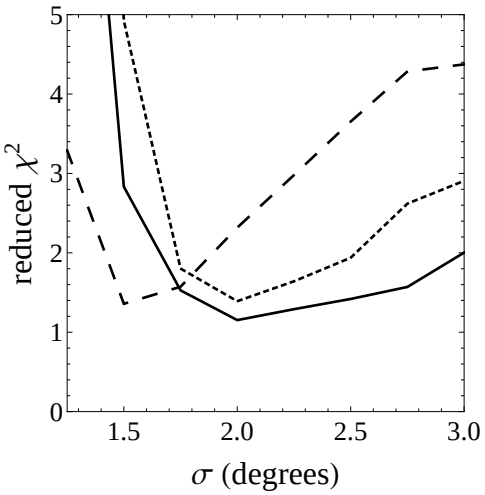


**Figure 5.** Reduced $\chi^2$ of the simulated-observed free inclination distribution of the cold component of the main belt compared to the real-observed free inclination distribution vs width of the inclination distribution ($\sigma$) for dotted: 42.4 to 43.8 au, dashed: 43.8 to 44.4, solid: 44.4 to 47.0 au. The minimum $\chi^2$ is for $\sigma$ of 1.5 to 2.0 degrees, and thus inclination distributions of $\sin(i)$ times a Gaussian (uniformly distribution around the forced plane predicted by the secular dynamics from the 4 giant planets) provide completely acceptable fits to the detections.

objects from a characterized sample to differentiate among non-rejectable widths. However, OSSOS has now produced a large enough characterized sample to determine the 'best fit' inclination width.

From Figure 4, which shows which forced planes are allowed based on the $i, \Omega$ distribution, it is clear that the allowed forced planes vary with the width of the inclination distribution, ($\sigma$). The $q, p$ distribution (Figure 3) is not so sensitive to the width of the inclination distribution (as the KS test is most sensitive to the center of a distribution and somewhat less sensitive to that distribution's shape), and allows a greater range of $\sigma$. It is the $i, \Omega$ distribution which is most sensitive to whether the width of the inclination distribution is too narrow or too wide. For example, for $a$ = 42.4-43.8 and 43.8-44.4 au, both inclination widths of $1.25^o$ and $2.25^o$ have $q, p$ distributions that allow forced planes near the expected forced plane, but the $i, \Omega$ distribution fails. Specifically, it is the $i$ distribution that determines if a given forced plane is rejected or not. For all of these survey simulations, the $\Omega$ distribution is only rejectable if the $i$ distribution is also rejectable. This permissiveness of the $\Omega$ distribution is a consequence of the fairly flat shape of this distribution over a wide range of proposed forced planes. This means the $\Omega$ cumulative distribution doesn't change too much and the KS test yields a non-rejectable value.

Given that the 'expected' (computed from the four giant planets) forced plane is generally non-rejectable, we now consider what width of the inclination distribution works best assuming that the expected forced plane is the true forced plane. Figure 5 shows a $\chi^2$ test of how well the survey simulated free inclination distribution matches the observed inclination distribution for different inclination widths ($\sigma$ in Eqn 5). As done earlier, we only consider TNOs with $i_{free} < 4^o$ in this fit. From this figure it is apparent that the cold population is best fit by an inclination width near $1.75^o$. The 43.8 to 44.4 au semi-major axis bin, where the CFEPS L7 kernel (Petit et al. 2011) is located, prefers a slightly lower inclination width but all three bins are satisfactorily represented by $\sigma = 1.75^o$,

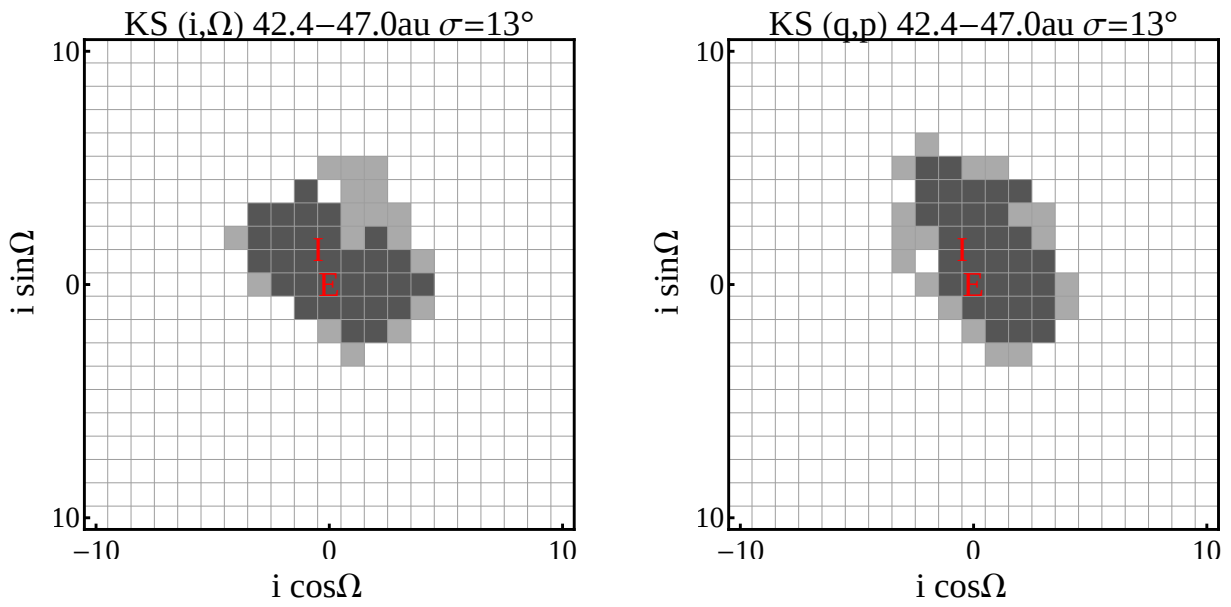


**Figure 6.** Acceptable forced planes derived from the hot population over the semimajor axis range 42.4–47.0 au, with $i > 9^o$ relative to the proposed forced plane. Left: bootstrapped statistic based on the $i$ and $\Omega$ distributions. Right: similarly for the $q$ and $p$ distributions. The hot population of the main Kuiper Belt does not provide any additional constraint on which forced planes are non-rejectable. Note that the scale of these figures is much wider than for Figures 3 and 4. Any bootstrapped statistic above 0.05 displays as dark grey, bootstrapped statistics between 0.05 and 0.01 are light grey. The ecliptic (E) and invariable plane (I) are marked in red. The location of the expected forced plane varies appreciably over this range of semimajor axes so we do not mark it on this figure.

which we thus adopt. Although it is possible that the dynamical kernel is indeed more concentrated, more data would be required to prove this.

A narrow width of the inclination distribution limits how much the cold population has been stirred. For example, imagine that a TNO starts with zero free inclination. If the planetary configuration changes suddenly, the TNO's forced inclination will also change suddenly. This induces a free inclination equal to the vector-difference between the new and old forced inclinations. Batygin et al. (2011) suggests it is possible to keep the inclination excitement to reasonable levels during the late stages of migration by controlling the $g_8$ precession rate (primarily controlled by the locations of Neptune and Uranus). Regardless of that, in models of hot object emplacement, the narrow width of the cold population is a very strong constraint that the vertical velocity kicks must have been very low.

### 3.2. *The Hot Population*

As discussed above, there is both a cold population and a hot population in the mid Kuiper Belt. We isolated the cold population by only considering TNOs within $4^o$ of each proposed forced plane. Similarly, we isolate the hot population by considering only TNOs that are more than $9^o$ from each proposed forced plane (we also tried cutting at $7^o$ and did not get substantially different results).

Due to the lower number of real detections to compare against, splitting into the three semi-major axis bins used for the cold population yields no constraints on the forced plane. When these bins are amalgamated into one (42.4 to 47 au), the forced plane is constrained, but it is a laxer constraint (see Figure 6). The forced planes allowed using only the hot population are consistent with the results

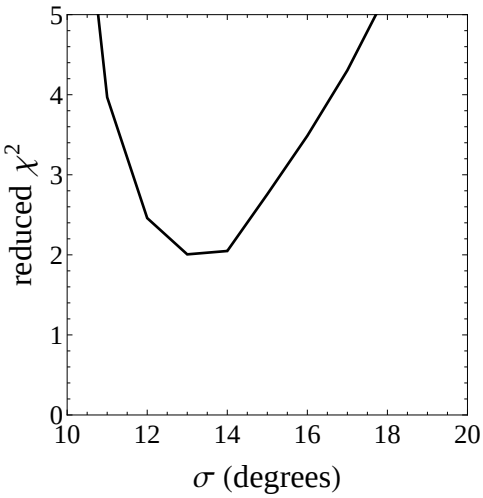


**Figure 7.** Reduced $\chi^2$ vs width of the inclination distribution ($\sigma$) of the hot main belt population for 42.4 to 47.0 au. The poorer quality of fit is likely caused by the assumption of a single forced plane over the entire range; see text for discussion.

from the cold population, but the lax constraint from the hot population means that we do not glean any additional information from the hot population on what forced planes are ultimately allowed versus the constraints we have from the cold population.

Like for the cold classicals, we ran a set of survey simulations using a forced plane equal to the expected forced plane for the middle of the bin (here 44.7 au) with a variety of widths for the inclination distribution ($\sigma$ in Eqn 5). We then calculate the goodness of fit of the inclination distribution. As done earlier, we consider here only TNOs with $i_{free} > 9^o$. As can be seen in Figure 7, the best fit width for the hot population is $\sim 13^o$, but $14^o$ is nearly as good. That said, the fit quality is somewhat worse than for the cold classicals. Part of the reason for this less-good fit is because we lumped all the hot classicals from 42.4 to 47 au into one bin, and performed survey simulations with only one $q_0$,$p_0$ for the forced plane; in reality the expected secular forced plane changes noticeably over the 42.4 to 47.0 au range used. Alternatively, the relatively poorer fit here may also hint that the inclination distribution for the hot classical population is not well fit by a simple inclination distribution of the form in Eqn 5. We however did not explore alternates to Eqn 5, as we feel a larger number of hot classical TNOs would be required to clearly differentiate between different shapes of the inclination distribution.

## 4. THE OUTER KUIPER BELT

The outer Kuiper Belt stretches outwards from the 2:1 resonance with Neptune. In this region, the expected secularly forced plane rapidly asymptotes towards the invariable plane (see Figure 1). Figure 8 shows our results for allowed forced planes using TNOs with $a$ = 50 - 80 au (57 objects), and Figure 9 shows our results for 48 - 150 au (83 objects), assuming the width of the inclination distribution ($\sigma$ in Eq. 5) is $17^o$ (see Figure 11 and discussion on the width of the inclination distribution for this population later in this section for why we chose this value of $\sigma$). In both cases, we consider all non-resonant TNOs in the specified (barycentric) semimajor axis bin. The survey simulations here used a single power law of slope 0.8 for the $H$ magnitude distribution, had semimajor axes drawn uniformly over the specified range, and had perihelion distances drawn uniformly from 34.0 to 50 au.

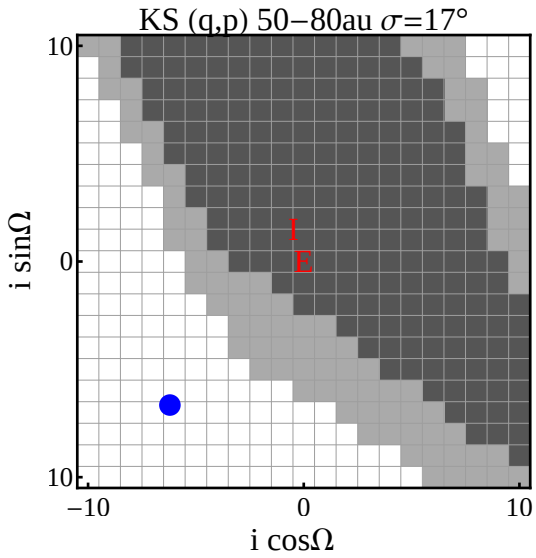


**Figure 8.** Bootstrapped statistics based on the joint $q$ and $p$ distributions for 50-80 au, non-resonant TNOs, with $\sigma = 17^o$. Any bootstrapped statistic above 0.05 displays as dark grey, bootstrapped statistics between 0.05 and 0.01 are light grey. The blue dot is Volk et al. (2017)'s nominal result for 50-80 au. The observed sample is consistent with the mean plane being the invariable plane, and inconsistent with the nominal result of Volk et al. (2017). See the text for more details.

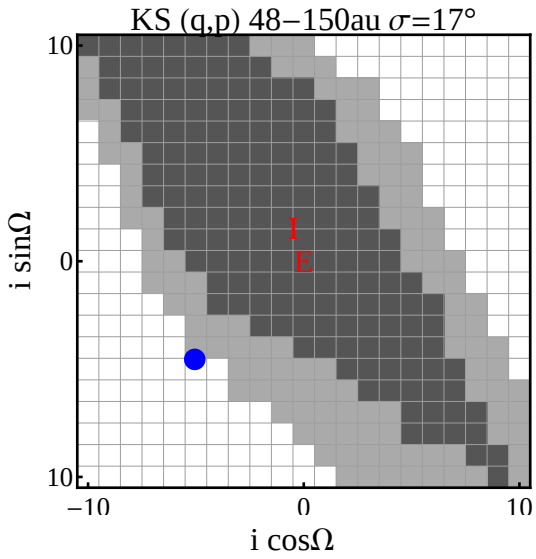


**Figure 9.** Bootstrapped statistics based on the joint $q$ and $p$ distributions for 48-150 au, non-resonant TNOs, with $\sigma = 17^o$. Any bootstrapped statistic above 0.05 displays as dark grey, bootstrapped statistics between 0.05 and 0.01 are light grey. The blue dot is Volk et al. (2017)'s nominal result for 50-150 au. The observed sample is consistent with the mean plane being the invariable plane, and rejects at 99% confidence the *nominal* result of Volk et al. (2017). See the text for more details.

To check if our results depend on the $H$ magnitude distribution we ran sets of survey simulations with the best fit 'knee' distribution from Lawler et al. (2018), having a bright slope of 0.9, with a

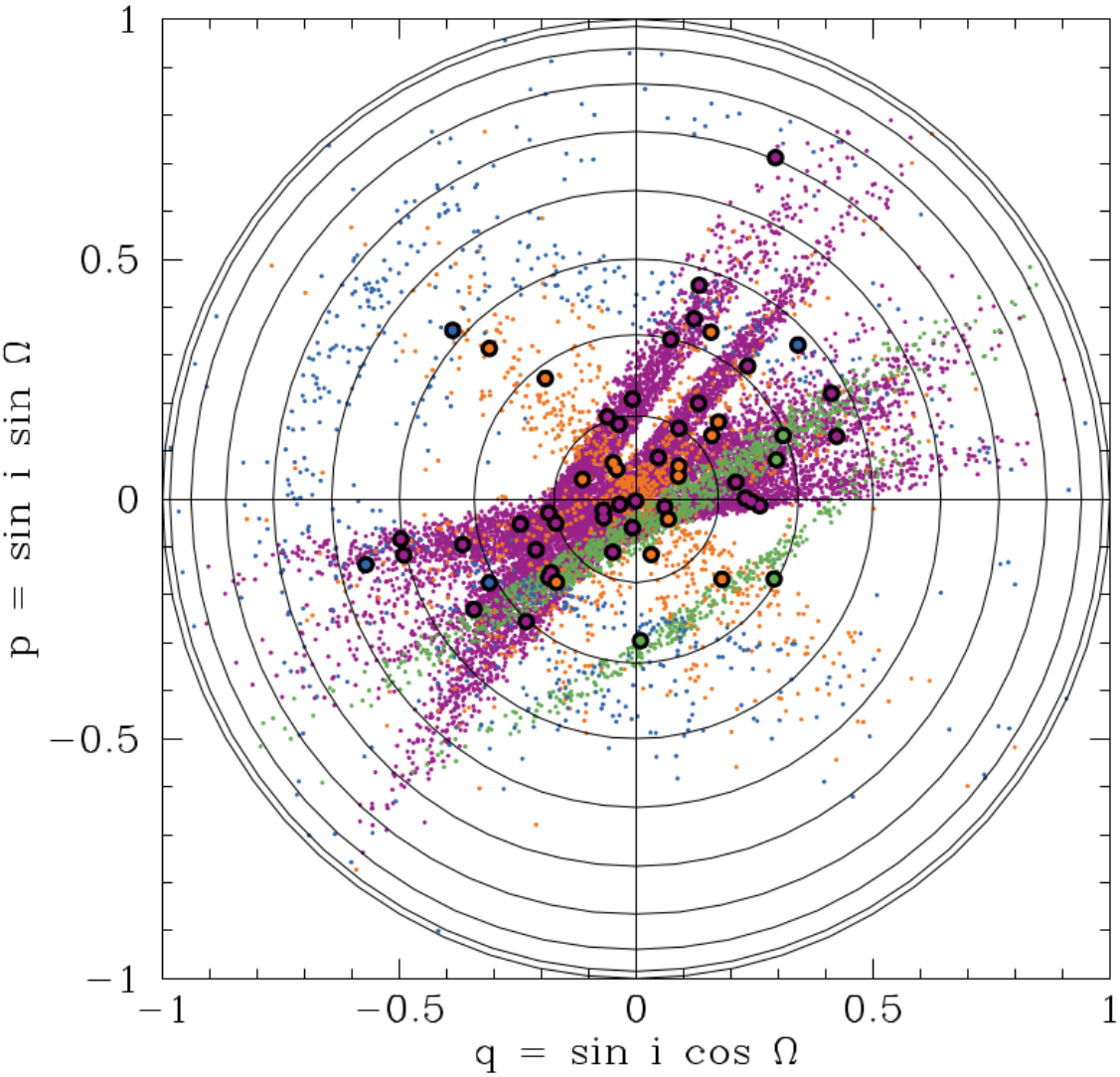


**Figure 10.** An example simulation of survey observations of populations for 50-80 au, where the forced plane is the invariable plane and the underlying inclination distribution is has a width of $17^o$. Small points are simulated observed objects, large circles are real observed objects. Each point is coloured by their observational survey: OSSOS in purple, CFEPS in orange, Alexandersen et al. (2016) in green, and HiLat in blue.

knee at $H = 7.7$ to a faint slope of 0.4. This choice slightly alters the proportion of objects detected by each of the surveys, but did not have any impact on which forced planes are rejectable.

We also checked if the distribution of perihelion distances would make a difference to our results by running a set of survey simulations with all TNOs' perihelia equal to 34 au. This extreme case also did not significantly affect the rejectability of various forced planes.

The layout of the entire set of non-rejectable regions in Figures 8 and 9 is a result of an observational sensitivity (or lack thereof) in the different $q, p$ quadrants. Consider Figure 10, which shows $q = \sin i \sin \Omega$ and $p = \sin i \cos \Omega$ of survey simulated detections and real detections. Surveys with pointings at low ecliptic latitudes (like CFEPS and OSSOS) find distant moving objects that are crossing the ecliptic at the observed longitude. A TNO going 'up' (from below the ecliptic to above

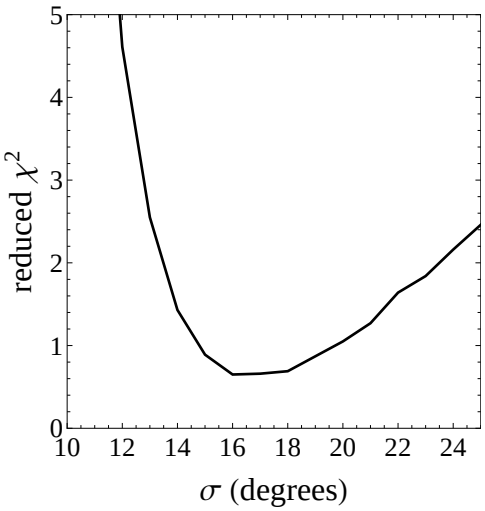


**Figure 11.** Reduced $\chi^2$ vs width of the inclination distribution ($\sigma$) of the outer Kuiper Belt (50-80 au). A 17 degree width around the invariable plane is a good match to the free inclination distribution.

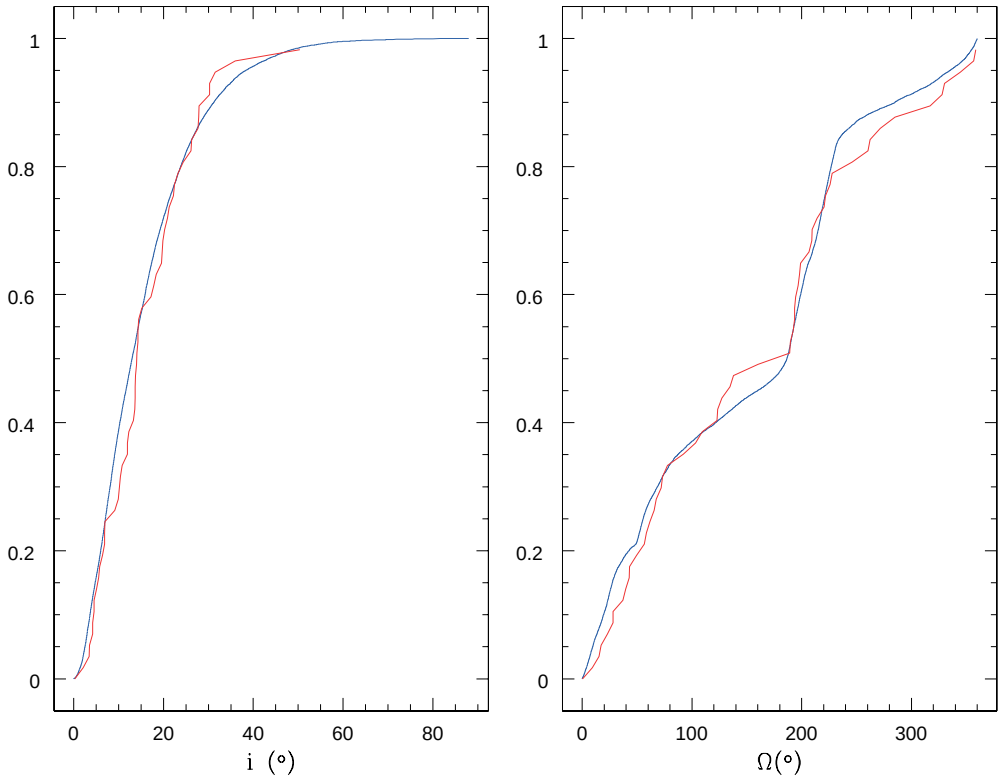


**Figure 12.** Cumulative distributions for the inclination and longitude of node for the survey simulation shown in Figure 10 (50 – 80 au, $\sigma = 17^o$, invariable as the forced plane). Blue shows the simulated-observed TNOs, red shows the observed TNOs. This model is not rejectable, with a KS statistic of 0.198 for the joint $q, p$ distributions and of 0.42 for the joint $i, \Omega$ distributions.

the ecliptic) will have its ascending node ($\Omega$) at the observed longitude, while a TNO going 'down' will have its descending node there. There is no bias favouring TNOs going 'up' versus those going 'down' (or vice versa), so low latitude surveys populate linear rays on Figure 10 that originate from (near) the origin. Surveys with pointings at higher ecliptic latitudes (like the high latitude block of Alexandersen et al. 2016) also make rays, but these rays are centered off the origin. In such high latitude surveys, the lowest inclination TNO that is observable has inclination equal to the minimum latitude of the pointing. Assuming the survey is north of the ecliptic and orbits are not too non-circular, the lowest-$i$ TNO would have an ascending node $90^o$ behind the observed longitude. For southern latitudes, the lowest-$i$ TNO would have an ascending node $90^o$ ahead of the observed longitude. Higher-$i$ TNOs that are observed have their ascending nodes shifted ahead or behind the lowest-$i$ case. The higher a TNO's inclination, the more its ascending node needs to be shifted from the lowest-$i$ case. Future similar-depth surveys like LSST will provide detections in the upper-left and lower-right $q, p$ quadrants, which will improve our ability to test forced planes in those directions.

The pointings of the OSSOS blocks give us strong sensitivity to ascending nodes in the lower left and upper right $q, p$ quadrants. While CFEPS (Petit et al. 2011), HiLat (Petit et al. 2017), and Alexandersen et al. (2016) add some coverage in other quadrants, these surveys were either not as deep or did not cover as much sky. There are approximately as many real objects in the lower left quadrant as in the upper right, and this feature is what makes forced planes in the lower left or upper right of Figures 8 and 9 fail. However, putting the forced plane in the upper left or lower right is consistent with the observed symmetry, making such forced planes non-rejectable by the suite of surveys we have available.

The most important test is to determine if we can reject the invariable plane as the center of the distribution (that is, the expected result if the particle precession is dominated by the four known giant planets). We are unable to do so; the invariable plane is perfectly acceptable as a mean plane given the suite of data sets we use, for both sets of semimajor axis ranges. The reduced chi-squared of the inclination distribution is less than one for the best-match model (Figure 11), and the match of the inclination and nodal longitude distribution is also excellent (Figure 12). We cannot reject the null result: this data set provides no compelling evidence against the invariable plane being the mean plane beyond Neptune (out to 150 au at least).

Assuming the real forced plane is the invariable plane, Figure 11 shows the goodness of fit for the observed inclination distribution versus width $\sigma$ (Eqn 5). Inclination widths that are too narrow overproduce TNOs with low inclinations, whereas a larger width puts too many TNOs in the high-$i$ tail. We find that the best-fit inclination width is $17^o$, indicating (albeit weakly) that this distribution is perhaps wider than for the hot classicals (where the preferred width is $14^o$; Figure 7). As can be seen in Figure 12, the cumulative distributions of $i$ and $\Omega$ for $\sigma$ of $17^o$ match very well with what is observed. While the difference in nominal width for the hot classicals and outer non-resonant populations is intriguing, this result is not conclusive proof that the outer Kuiper Belt has a different width than the hot main belt. From Figures 7 and 11, a width of $\sim 15^o$, for example, is acceptable for both of these populations.

### 4.1. *Constraints on Additional Planets*

Volk et al. (2017) found that, using the Brown & Pan (2004) method, the MPC sample of TNOs indicates that the forced plane for $a$ = 50-80 and 50-150 au is in the lower left $q, p$ quadrant. Their uncertainty in the forced plane was moderately large, though they found it to be inconsistent with the

invariable plane at $> 95\%$ confidence. Using a largely independent data set and a different analysis method we do not reproduce this rejection of the invariable plane, which we instead find completely acceptable. Our results rule out the nominal forced plane derived for the $a$=50–80 au MPC sample at $> 99\%$ confidence (Figure 8), and most of the lower left $q, p$ quadrant that said nominal forced plane lies in. The 50–150 au sample's nominal forced plane derived with the Brown & Pan (2004) method is rejected at $> 99\%$ confidence by our method applied to the OSSOS sample, but lies near a region that we can reject at only at 95% (Figure 9). There is no compelling evidence from the analysis of the independent data set that a warp in the direction and amplitude found by Volk et al. (2017) is preferred, although we cannot rule out smaller warps in that direction. Our result is that the expected invariable plane is consistent with the OSSOS data set.

Given the tension between the results Volk et al. (2017) and the results presented here, one could ask where the difference between our conclusions could come from. One possibility is that the set of TNOs Volk et al. (2017) were working with, from the Minor Planet Center (MPC) database, contains systematically incomplete object reports from some surveys. The Brown & Pan (2004) method cannot correctly derive the true forced plane with an incompletely reported data set; it assumes that all TNOs discovered in the survey have had orbits reported. So if some survey(s) did not report all TNOs they discovered to the MPC before Volk et al. (2017) did their analysis, then Volk et al. (2017) would be working with an incomplete data set. For example, several TNOs appeared after the Volk et al. (2017) analysis in Minor Planet Electronic Circulars[2], but several other TNOs from the same dark run had been reported to the MPC prior to the Volk et al. (2017) analysis. This is interesting especially because these three newly reported TNOs have large inclinations and ascending nodes in the *opposite* half space of the warp derived by Volk et al. (2017). Incomplete reporting happens for a large variety of reasons, but in this context it means that the set of MPC objects cannot be taken at face value. A final resolution of the tension between these two results for the $a$=50–80 au sample will require complete data sets, but because we know that the OSSOS data set is calibrated and complete we have reasonable confidence in our model rejection estimates.

Constraining the presence of an additional planet from these results is tricky given the large range of TNO semi-major axes considered here, in particular because the forcing plane varies as a function of the TNO's semi-major axis (see Section 2.1). In the presence of an additional planet in the $\sim$100 au region, this dependence would be quite dramatic for the TNOs considered here. It is also reasonable to assume that with this additional planet present, the width of the inclination distribution would change as a function of semi-major axis, and is perhaps not at all well described by Eqn 5. For example, if these TNOs are put in place via scattering or resonant interactions with Neptune, they would start symmetrically distributed about Neptune's mean plane. As time progressed, these TNOs would subsequently precess around the forced plane dictated by their new semimajor axis, which in the presence of an additional planet would not be the invariable plane. Such an emplacement would give the TNO inclination distribution a dependence on TNO semimajor axis. While it is true that our analysis indicates the inclination distribution may be wider for the outer Kuiper Belt than for the hot main classical belt, as would be expected from such a situation with an additional mass, the difference in these populations' inclination widths is not statistically significant enough to be viewed as evidence of an additional planet in the $\sim$ 100 au region.

[2] Minor planet electronic circulars 2018-K-118, 2018-K-119, and 2018-K-120 reporting the discoveries/orbital determination of TNOs 2015 FK172, 2015 KG172, and 2016 FX58.

With regards to more distant planets, possible planets at several hundred au will not strongly affect the forced plane for TNOs with semi-major axes below ∼100 au. For example, Batygin & Brown (2016)'s "Planet 9" is too distant to cause a warp in the mean plane at these distances. A 10 Earth-mass planet with a semi-major axis of ∼700 au, and inclined at $30^o$ doesn't pull the expected forced plane more than a degree off the invariable plane until about $a = 130$ au[3]. Only if the planet is at the closer, more massive, and higher inclination end of those ranges does it significantly pull the expected forced plane away from the invariable at ∼100 au.. (This is, of course, why Volk et al. (2017) postulated a closer, smaller planet.)

## 5. CONCLUSIONS

We make use of characterized surveys via the survey simulation technique to determine the forced plane of the main classical trans-Neptunian belt and the outer trans-Neptunian belt. Everywhere we look, the expected forced plane from secular theory is consistent with the observed sample.

The forced plane of the cold main belt is constrained to be within $\sim 0.5^o$ of that expected from secular theory. In the outer belt, our results again are consistent with the predictions of secular theory. The nominal warp found by Volk et al. (2017) is strongly ruled out, though a mild warp in that general direction is still possible. We cannot rule out dramatic warps in directions we are not sensitive to with OSSOS (Bannister et al. 2016, 2018), CFEPS (Petit et al. 2011), Alexandersen et al. (2016), and HiLat (Petit et al. 2017). Our results do not indicate the presence of an additional Mars-mass planet within ∼100 au, as distributing TNOs with $a = 50$–$150$ au about the invariable plane provides a good match to observations from the characterized surveys we use. The results are robust against changes in the $H$ magnitude distribution (i.e. the size distribution), and in the distribution of perihelion distance. The purported 'Planet 9' (Batygin & Brown 2016) is too distant to affect the TNOs we consider.

Assuming the true forced plane is that expected from secular theory and assuming an underlying inclination distribution of the form found in Eqn 5, we find that the inclination distribution of the cold classical main belt is very narrow, with a best fit width of $\sim 1.75^o$. Such a narrow width implies that this population was not much disturbed as the giant planets migrated. The best fit width of the hot main belt population is $\sim 14^o$. The outer trans-Neptunian belt (50 – 80 au) is very well fit with width $\sim 17^o$.

CVL acknowledges funding from the NSERC CREATE grant Technologies for Exo-Planetary Science (TEPS). MTB appreciates support from UK STFC grant ST/P0003094/1.

## REFERENCES

Adams et al 2014, AJ, Volume 148, article id. 55, 17 pp.

Alexandersen, M., Gladman, B., Kavelaars, J. J., Petit, J.-M., Gwyn, S. D. J., Shankman, C. J., Pike, R. E. 2016, AJ, 152, article id. 111, 24 pp.

Bannister, M. et al. 2016, AJ, 152, article id. 70, 25 pp.

Bannister, M. et al. 2018, ApJS, 236, article id. 18, 19 pp.

Batygin, K., Brown, M. E., Fraser, W. C. 2011, ApJ, 738, article id. 13, 8 pp.

[3] We tried a variety of values for the hypothetical very distant planet: $a$ of 400-700 au, mass of 5-10 Earth-masses, $i$ of 5-30$^o$. We found that in most cases the additional distant planet starts making a $> 1^o$ difference from the otherwise-expected invariable plane after ∼120 au

Brown, M. 2001, AJ, 121, pp. 2804-2814.

Brown, M. E. & Pan, M. 2004, AJ, 127, 2418-2423

Batygin, K. & Brown, M. 2016, AJ, 151, article id. 22, 12 pp.

Chiang, E. & Choi, H. 2008, AJ, 136, 350-357

Dawson, R. I. & Murray-Clay, R. 2012, ApJ, 750, article id. 43, 29 pp.

Elliot, J. L., Kern, S. D., Clancy, K. B., Gulbis, A. A. S., Millis, R. L., Buie, M. W., Wasserman, L. H., Chiang, E. I. and Jordan, A. B., Trilling, D. E., Meech, K. J. 2005, AJ, 129, 1117-1162

Gulbis, A.A.S. et al. 2010, AJ, 140, pp. 350-369

Jones, R.L. et al. 2006, Icarus 185, p. 508-522.

Kavelaars, J.J. et al. 2009, AJ, 137, pp. 4917-4935.

Lawler, S. et al. 2018, AJ, 155, article id. 197, 9 pp.

Lawler, S. et al. 2018, Frontiers in Astronomy and Space Sciences, 5, id.14

Murray, C.D. & Dermott, S.F. 1999, Cambridge UP, Cambridge

Petit, J.-M., Kavelaars, J. J., Gladman, B. J., Jones, R. L., Parker, J. W. Van Laerhoven, C., Nicholson, P., Mars, G., Rousselot, P., Mousis, O., Marsden, B., Bieryla, A., Taylor, M., Ashby, M. L. N., Benavidez, P., Campo Bagatin, A., Bernabeu, G. 2011, AJ, 142, pp 131

Petit, J.-M., Kavelaars, J. J., Gladman, B. J., Jones, R. L., Parker, J. Wm., Bieryla, A., Van Laerhoven, C., Pike, R. E., Nicholson, P., Ashby, M. L. N., Lawler, S. M. 2017, AJ153, article id. 236, 11 pp.

Pike et al. 2017, AJ, Volume 154, article id. 101, 8 pp.

Saverio, & Malhotra, R. 2018, AJ155, article id. 143, 10 pp.

Schwamb, M. E., Brown, M. E.; Rabinowitz, D. L., Ragozzine, D., 2010, ApJ, 720, pp. 1691-1707

Schwamb et al. 2018, arXiv:1809.08501

Volk, K. & Malhotra, R. 2017, AJ, 154, pp 62